Check for updates

Shape memory meta-laminar jamming actuators fabricated by 4D printing

Mohammadreza Lalegani Dezaki [ID] and Mahdi Bodaghi [ID] *

Laminar jamming (LJ) technology is a hot topic because it allows for the transition from conventionally quick, precise, and high-force rigid robots to flexible, agile, and secure soft robots. This article introduces a novel conceptual design of meta-laminar jamming (MLJ) actuators with a polyurethane shape memory polymer (SMP)-based meta-structure fabricated by 4D printing (4DP). The sustainable MLJ actuators behave as soft/hard robots *via* hot and cold programming accompanied by negative air pressure. The advantage of MLJ actuators over conventional LJ actuators is that a continuous negative air pressure is not required to stimulate the actuator. SMP meta-structures with circle, rectangle, diamond, and auxetic shapes are 4D printed. Mechanical properties of the structures are evaluated through three-point bending and compression tests. Shape memory effects (SMEs) and shape recovery of meta-structures and MLJ actuators are investigated *via* hot air programming. MLJ actuators with auxetic meta-structure cores show a better performance in terms of contraction and bending with 100% shape recovery after stimulation. The sustainable MLJ actuators have the capabilities of shape recovery and shape locking with zero input power while holding 200 g weight. The actuator can easily lift and hold objects of varying weights and shapes without requiring any power input. This actuator has demonstrated its versatility in potential applications, such as functioning as an end-effector and a gripper device.

1. Introduction

Soft robots are amenable to human interaction and environmental adaptation. They can securely interact with bodies and move across dynamic settings, thanks to their compliance.[1,2] One of the most common procedures to build soft robots is 4D printing (4DP) technology using fused deposition modelling (FDM).[3,4] The development of 4D-printed adaptive and dynamic metamaterials is facilitated by the incorporation of life into 3D-printed items with a time dimension.[5,6] Mechanical metamaterials have exceptional qualities that do not exist in natural materials because of the periodic arrangement of bespoke artificial microstructural units.[7] Thanks to their exceptional qualities, mechanical metamaterials have been applied in several research and engineering domains.[8] These adaptive and dynamic actuators are constructed from a variety of smart materials like shape memory polymers (SMPs) and shape memory alloys.[9,10] Soft actuators are divided into numerous subgroups such as fluidic-driven,[11,12] thermo-driven,[13,14] electro-driven,[15,16] pH-driven,[17] light-driven,[18] and magneto-driven actuators.[19,20]

Soft actuators made from 4DP technology have been widely used in different industries from manufacturing to biomedical sectors.[21] Soft robots offer certain benefits, such as being lightweight and allow for safe human–robot contact, but they also have some drawbacks, such as poor motion control, high power consumption, and low output forces/torques.[22] The use of variable stiffness actuators is a practical technique to provide robots with the benefits of both rigid and soft architectures.[23] Jamming structures are promising for variable stiffness control because of their simplicity, low cost, adaptability, quick reaction, and ability to be customised.[24]

Jamming is one such enabling technique that involves the evacuation of fluid-tight envelopes containing different materials to bring the parts into touch with one another, create friction, and increase device stiffness.[25] A vacuum bag and internal components encased in the vacuum bag are the typical components of jamming constructions. Large normal forces between internal parts are produced when a vacuum pressure is applied, and the resulting frictional forces stop the jamming structure from deforming. The rigidity of the structure may be actively controlled by varying the pressure differential between the vacuum bag's inside and outside.[26] As a result of soft actuators' safety and simplicity of control, jamming structures have been frequently used to improve their stiffness.[27]

In recent years, jamming strategies based on various internal parts have been investigated.[28,29] A flexible yet inextensible sheet is the most common internal component used in laminar jamming (LJ) designs. They typically respond quickly by utilising a suction system and are typically lightweight. Other innovative

Department of Engineering, School of Science and Technology, Nottingham Trent University, Nottingham, NG11 8NS, UK. E-mail: mahdi.bodaghi@ntu.ac.uk

This journal is © The Royal Society of Chemistry 2023

jamming structures, including particles and LJ, have also lately been developed.[30] Narang et al.[31] created an analytical and finite element model that quantitatively described the behaviour of two-layer pneumatic jamming structures during all significant deformation stages. The integration of jamming structures into soft machines allows them to selectively display the stiffness, damping, and kinematics typically associated with traditional rigid robots. Lin et al.[32] developed origami skeletons with controllable stiffness for compact and versatile artificial muscles. The strategy of combining origami folding and adjustable stiffness, which was inspired by the human limb's activity strategy, was used to create controllable stiffness origami skeletons. The actuators were based on the LJ and origami folding of multiple layers of a flexible sandpaper, for a common mono-functional single-morphing vacuum-powered cube-shaped artificial muscle.

Kwon et al.[33] created a sandwich jamming structure that consists of a rubber-laminated front sheet and an anisotropic cellular core. When the structure was not jammed, the light anisotropic core's low bending modulus allowed for excellent structural compliance, but when jamming occurred, it became extremely stiff. The structure offered a better strength-to-weight ratio and stiffness change ratio between the unjammed and jammed states as compared to particle and LJ structures. Wang et al.[34] developed a tendon-driven soft robotic hand with variable stiffness using an LJ structure. The single tendon driver controlled the deformation while the LJ structure independently adjusted the stiffness of the actuator components.

Narang et al.[35] showed that LJ, a beneficial variable-impedance mechanism, overcame several limitations of conventional variable dampers. It was demonstrated that although the variable-damping qualities of jamming structures allow oscillation amplitudes, decay rates, and steady-state deformations to be set on demand, the variable-stiffness properties of jamming structures allowed oscillation frequencies to be tuned. Also, the results showed that the impact response of soft structures with built-in jamming mechanisms could be adjusted to either save or release energy as required. Gerez et al.[36] created a hybrid, soft, robotic exoskeleton glove with all fingers capable of abduction using the LJ technique. A telescoping additional thumb that improved grasp stability, and soft structures with variable stiffness at the glove's back that could change the finger bending profiles and help stabilise the desired grasping pose were developed. The user's gripping abilities were significantly improved by the hybrid assistive, exoskeleton glove, which could apply the pressures necessary to carry out a variety of daily chores. Also, Willemstein et al.[37] printed a soft actuator by a coiling liquid rope and the infill foam approach for printing structures with variable porosities.

Mohammadreza Lalegani Dezaki received his MSc degree in Manufacturing Systems Engineering from Universiti Putra Malaysia (UPM). He has published several papers in the field of 3D/4D printing and soft actuators. In 2021, He was awarded a PhD studentship issued by Nottingham Trent University (NTU). His current research interests involve the design and development of smart soft actuators for soft robots.

Mohammadreza Lalegani Dezaki

Dr Mahdi Bodaghi (BSc, MSc, PhD, PGCAP, FHEA, CEng, MIMechE) is a Senior Lecturer in the Department of Engineering at Nottingham Trent University. He is also the founder and leader of the 4D Materials & Printing Lab that hosts a broad portfolio of projects focusing on the electro-thermo-mechanical multi-scale behaviours of smart materials, soft robotics, and 3D/4D printing technologies. His vast experience and research on smart materials and additive manufa-

Mahdi Bodaghi

cturing has led him to co-found the 4D Printing Society and to co-edit the book series-Smart Materials in Additive Manufacturing. His research has also resulted in the publication of over 180 scientific papers in prestigious journals as well as the presentation of his work at major international conferences. Mahdi has also served as Chairman and member of Scientific Committees for 16 International Conferences, as Guest Editor for 10 Journals, as Editorial Board Member for 10 scientific Journals, and as Reviewer for over 150 Journals. Mahdi's research awards include the Best Doctoral Thesis Award of 2015, 2016 CUHK Postdoctoral Fellowship, the Annual Best Paper Award in Mechanics and Material Systems presented by the American Society of Mechanical Engineers in 2017, 2018 Horizon Fellowship Award, and 2021 IJPEM-GT Contribution Award recognized by the Korea Society for Precision Engineering.

The use of this grading allowed for the realisation of rectangular constructions with a variety of deformation patterns, including twisting, contracting, and bending.

The LJ actuator must be light and should not be heavy. Also, the actuator should be strong enough to endure the moment caused by external shocks. The actuator should be precise and accurate enough to fulfil the required task. A major challenge with pneumatic LJ actuators is that the negative pressure should be always working to hold the actuator in the required position. Energy consumption increases due to continuous stimulation to activate the actuator. Hence, a sustainable design can reduce power consumption accordingly.

In this paper, a novel method is proposed combining 4DP and LJ technology to produce soft/hard meta-laminar jamming (MLJ) actuators with shape recovery, shape locking, and zero-power holding features. The MLJ actuators are activated via hot programming and the shape-locking feature is achieved via cold programming accordingly. Designing MLJ actuators that behave differently when the structure is unjammed and jammed has not received much attention. A combination of 4DP and LJ technology allows us to develop sustainable laminar jamming sandwich actuators. The vacuum-based jamming is enhanced by using the shape memory effect (SME) of 4D-printed metamaterials to decrease energy consumption. The lightweight metamaterial core allows for excellent structural compliance and their SME allows for shape-locking the structure in the required position with zero power. The method has the advantage of improving reconfigurability and reusability by enabling the actuator behaviour to be switched while maintaining the same core design by simply adjusting the relative stiffness of the sleeve at various locations. Also, the power consumption of actuators is reduced due to the SME and locking system. The actuator's capabilities are shape locking in the required position, shape recovery, high stiffness, and bending and contraction. The actuators can be used in different applications such as lifting and gripping with zero power.

2. Materials and methods

2.1. Concept and model

This study builds on the knowledge of SMEs, LJ actuators, and FDM printing to construct the functionally graded metamaterial concept. The fundamental concept is to combine SMPs and LJ technology to provide prospects for designing and developing sustainable adaptive MLJ actuators. SMPs have the unique capability to change into a temporary shape upon being exposed to external stimuli, such as heat, and subsequently revert back to their original shape. The goal now is to carry out the programming procedure with MLJ technology. Fig. 1 depicts a typical diagram-based, step-by-step thermo-mechanical programming methodology for MLJ actuators.

At a low temperature below the transition temperature (T_g), where SMP metamaterial is stable in a glassy phase, it begins under a strain- and stress-free condition. Then, the temperature is raised over T_g. Negative pressure is used to provide the greatest amount of strain to SMP that is in the rubbery phase. The material is cooled to a low temperature while the vacuum pressure is maintained at a constant level. This stage involves accumulating inelastic stresses while the rubbery phase eventually transitions to the glassy phase. The structure is finally released while the material still has a pre-strain. The vacuum is cut off and the actuator remains in the position aligned with the meta-structure's shape. The actuator module is heated at a high temperature for activation, releasing tension and restoring the permanent form.

PVC films can be used inside the module to change the behaviour of the actuator from contraction to the bending form. Without PVC films, the actuator is contracted and compacted via negative air pressure. Under both conditions, the actuator's shape is locked until the temperature goes up again. It has been discovered that the metamaterial core in the MLJ actuator can create MLJ structures and impose inelastic pre-strain that may cause SMEs to manifest in a certain manner. It may be inferred that the metamaterial's shape
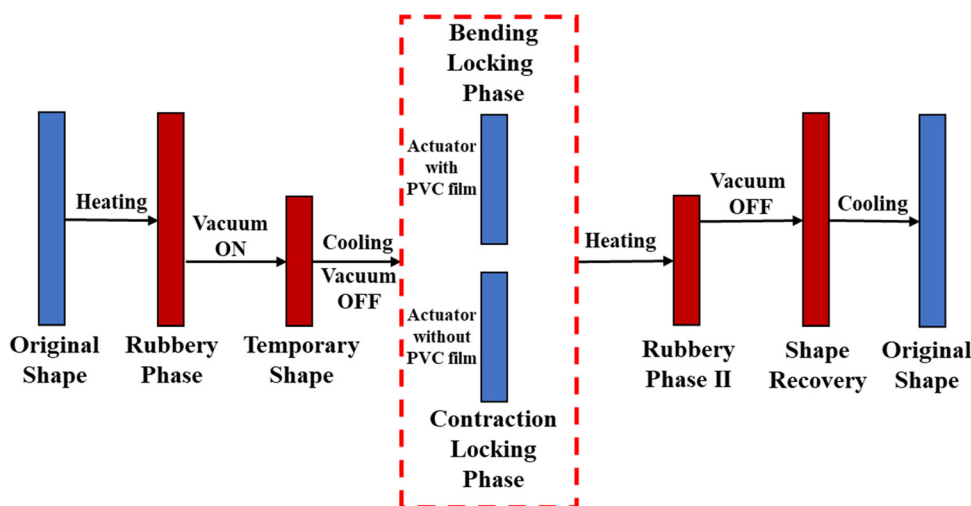

Fig. 1 Procedure and concept of activation of 4D-printed MLJ actuators.

may be programmed in numerous ways and a range of pre-strain values are obtained. Also, printing parameters, pressure values, material properties and structure size can be effective which need to be considered in MLJ actuators.

2.2. Design and fabrication

Metamaterials' deformability and energy absorption characteristics make them suitable in this case to be used as a core structure. Sandwich-enclosed MLJ actuators are the main aim of this study. The design of all structures is kept constant and similar. Five different lattice shapes are selected to examine their mechanical properties in MLJ actuators. Honeycomb shape, circle shape, rectangular shape, diamond shape, and auxetic shape structures are chosen to be designed in this study. These types of structures are preferred because they may be used in a variety of applications and have dependable mechanical characteristics. All models are developed in SolidWorks© software at a constant size and volume. The designs and their details are shown in Fig. 2. The size of all meta-structures are the same.

Polyurethane SMP-based filaments with a 1.75 mm diameter from SMP Techno. is used to print the core structures. The FDM method is used to carry out the printing process. FDM can print complex SMP structures according to specifications. Samples are produced from bottom to top using created pathways and G-codes using Slic3r software. An open-source 3D printer is used to build the core structures accordingly. The quality of printed SMP metamaterials is impacted by several printing factors.[4,38] The printing parameters used to build samples are 210 °C nozzle temperature, 0 °C bed temperature, 40 mm s^{-1} print speed, 0.2 mm layer height, and 5 mm retraction distance. The same settings are used to print all specimens.

The interior architectures of actuators are modelled using those of vacuum-actuated muscle-inspired pneumatics and fluid-driven origami-inspired artificial muscles, whereas the internal structural skeleton is more influenced by fluid-driven origami-inspired artificial muscle actuators. The procedure for building the MLJ actuators is shown in Fig. 3. The heating temperature is increased more than material T_g to activate the core structure. Hence, a heat-resistant nylon PA6 vacuum bagging film with a 200 °C maximum operating temperature from Easy Composite Ltd is used in this study. A heat sealer is used to seal 3 sides of the film. The core metamaterials are placed inside the bagging film. A thin PVC film with a size of 0.25 mm is used inside the actuator module to control the motion of the actuator. The location of the film can be varied based on motion requirements such as bending or contraction. A TPU tube is attached to the module from one side and polyisobutylene sealant tape from Easy Composite Ltd is used to seal the module accordingly. The actuator is activated in terms of contraction or bending to evaluate its performance.

2.3. Dynamic mechanical analysis (DMA)

Most polymers typically exist in a soft, above-glass transition temperature state, and in a hard, brittle state at ambient temperature. The dynamic mechanical analyser 8000 from PerkinElmer is used to test the storage modulus of polyurethane SMP. The sample for the DMA test is 3D printed at a speed of 40 mm s^{-1}, and its model measurements are 15 mm (length) × 1.6 mm (width) × 1 mm (thickness). The most important thermodynamic factor that contributes to the SME of SMPs is T_g, and, therefore, it should be studied to assess the shape memory behaviour of 4D-printed polyurethane. Additionally, it is
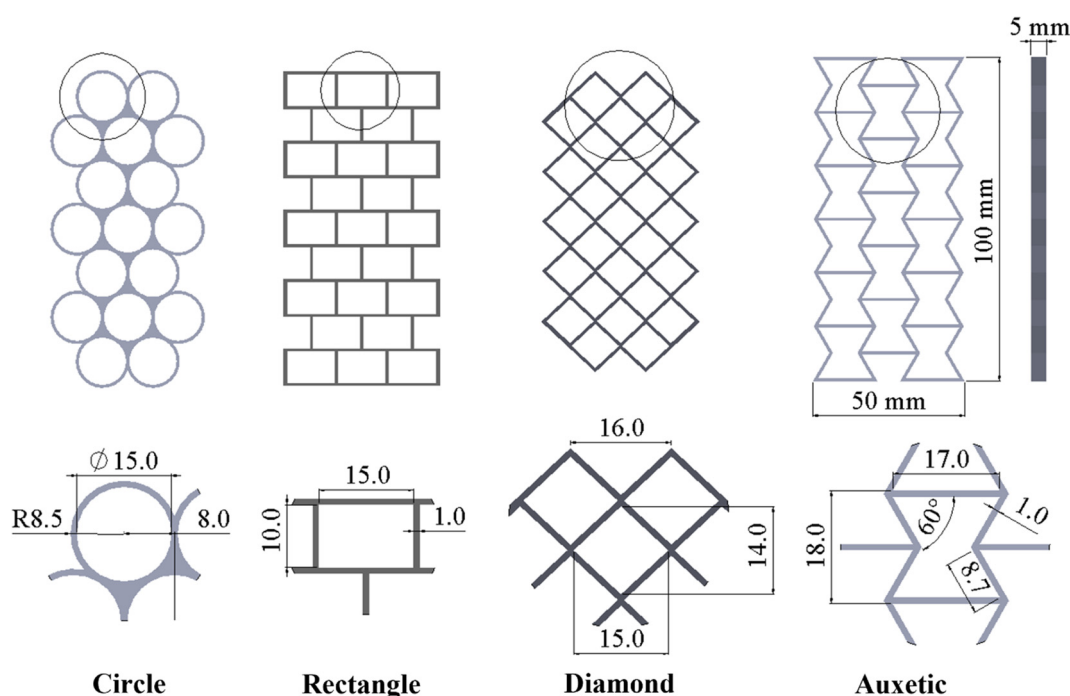

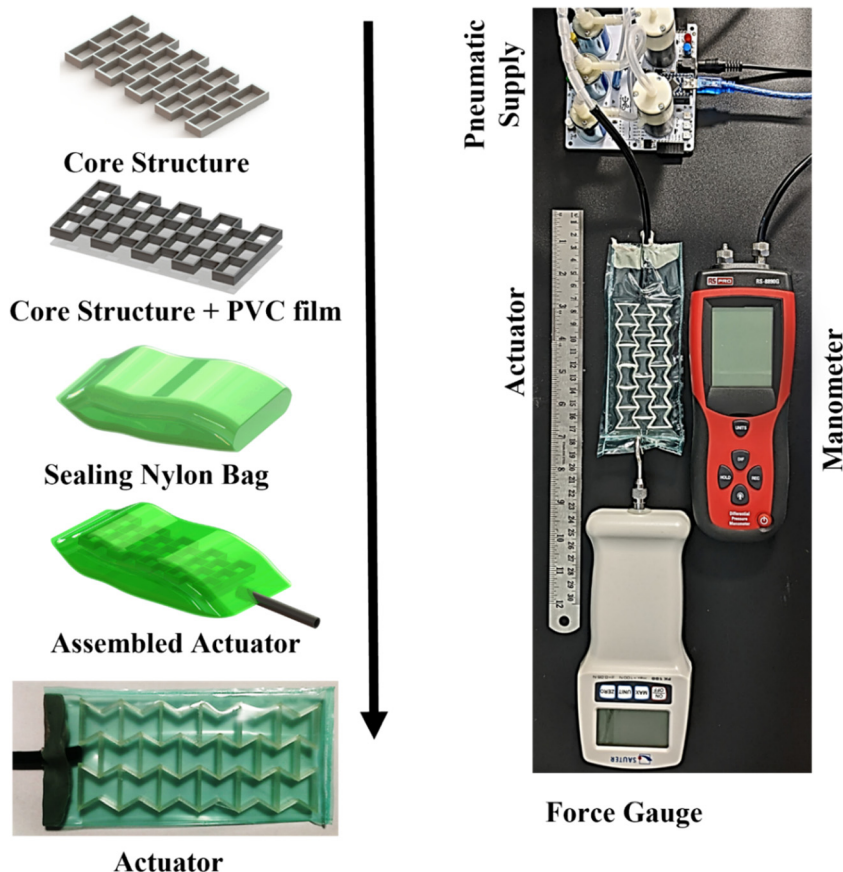**Fig. 2** 2D schematic design of meta-structure cores with details.

Fig. 3 Procedure of building MLJ actuators and equipment to investigate their performance.

important to describe how heating affects the T_g of the employed material. The chosen test frequency is 1 Hz, which corresponds to the gradual alteration in characteristics brought on by temperature. The DMA test sequence ramps from a starting temperature of 25 °C to 85 °C at a rate of 5 °C min^{-1}.

2.4. Mechanical properties

In this study, a three-point bending test is conducted to determine the stiffness and strength of MLJ actuators. To investigate their strength and behaviour, the test procedure for actuators is conducted for metamaterials, the actuator in the vacuum bag with and without PVC sheets. A Shimadzu AG-X plus machine (Shimadzu, Shimadzu UK, UK) is used and TRViewX (Shimadzu, Shimadzu UK, UK) records the data accordingly. Both sides of the samples are clamped to avoid any movements during the test. A force rate is applied, and the deflection is recorded continuously. The cross-head speed is set to 5 mm min^{-1} with a 1 kN load cell for the loading and unloading procedure. A set of three samples is examined for each test. Also, the effects of vacuum pressure on the flexural strength are evaluated to check the performance of the actuator accordingly. A flexural test is conducted to analyse the structures' properties and actuators' performance while the negative pressure is working continuously. Also, a compression test is conducted to investigate the behaviour of structures under load in terms of contraction in actuator modules. The width is

increased to 10 mm and the length of samples is reduced to have better stability in the compression procedure. A Shimadzu AG-X plus machine is also used in this experiment and TRViewX records the data accordingly. The cross-head speed is set to 5 mm min^{-1} for the loading and unloading procedure. A maximum of 10% strain is applied to all samples to achieve consistent results and avoid large deformation in the structures. The performance of structures and actuators is investigated at a high temperature which is above T_g. The previous procedures are repeated accordingly. The temperature is set to 70 °C at which the actuator starts to contract or bend. A heating chamber is placed for a three-point bending test and compression test. The upper jaw goes down when the temperature reaches 70 °C.

2.5. Shape memory effects

Research into the shape memory effect is carried out under bending and contraction conditions. Samples are heated from room temperature to 70 °C. Immediately after the loading, the samples are rapidly cooled to 25 °C. The samples are heated again to investigate the shape recovery time and ratio. Shape recovery values for metamaterials and MLJ actuators are determined after the free shape memory test in bending and contraction modes are repeated up to 3 times. First, the shape recovery ratio and time of meta-structures are investigated. Then, their SMEs are evaluated when they are used as a core structure in MLJ actuators. The shape recovery ratio is

calculated using formula (1) as follows:

$$\text{Recovery ratio}(\%) = \frac{\text{Height of actuator after recovery}}{\text{Initial height of actuator}} \times 100$$

(1)

2.6. Test measurement

The module should be sealed properly to avoid leakage. The soft actuators are operated using a programmable-air kit from Tinkrmind with a 1 bar maximum operating vacuum pressure. The kit can control the output flow from 0 to 1 bar. A differential pressure manometer is used to measure the negative pressure differences during the procedure. A heat gun is used to ensure that the structure is heated above its T_g. SME and shape recovery are evaluated by heating the structure to investigate the recovery time. An infrared camera from FLIR is used to assess how the 4D-printed metamaterial is behaving. An electronic force gauge with 100 N maximum force from SAUTER is used to measure the generated force from each actuator as shown in Fig. 3. The force gauge and actuators are clamped from one side to have consistent results. A video camera is used to record the actuator's motions and movements. Additionally, motion is captured and the trajectory route of soft actuators is provided using the PASCO programme.

3. Results and discussion

3.1. Three-point bending test

Fig. 4 displays the temperature-dependent outcomes for storage modulus and tan δ. The temperature is increased from 25 °C to 85 °C. Results show that the material exhibits a notable peak and fall in the tan δ, the storage module, and its limited glass transition range. Tan δ reaches a peak of 0.8 when the temperature goes beyond 55 °C and it sharply falls to 0.09 when the temperature passes 60 °C. The storage modulus is found to be approximately 1600 MPa in the glassy phase and dramatically decreases to 35 MPa in the rubbery phase after T_g. The materials

become rubbery, viscous liquids because of the chain flow, which also rapidly reduces their storage modulus and leads them to lose stiffness. $T_g = 60$ °C is indicated by a conspicuous peak in the tan δ graph. Hence, the temperature of activation should be higher than T_g. This feature helps the printed structure to recover its original shape after deformation on increasing the temperature.

Three-point bending and compression tests are performed at room temperature and 70 °C to forecast the mechanical behaviour of MLJ structures under different conditions. Since the actuators are bent through vacuum jamming, it is vital to find out the performance of core structures and their behaviour under the three-point bending test. The test is conducted to evaluate the behaviour of cells and structures. The test helps us to investigate the core structures' mechanical properties in terms of bending in actuator modules. The tests are repeated three times and the median results are reported accordingly. Fig. 5 shows the procedure of three-point bending tests of metamaterials and modules. The core structure is stiff under both jammed and unjammed conditions. A minimum cell thickness of 1 mm is assigned to improve the structural performance in terms of shape memory behaviour. Fig. 5(a) shows the procedures of bending tests on metamaterial structures alone.

The procedure starts with loading the samples up to 10 mm. Then, the structure is unloaded and the jaw goes back to its initial position accordingly. Fig. 5(b) illustrates the module which has a core structure, PVC sheet, and vacuum bag. Meanwhile, Fig. 5(c) shows the module that has a core lattice structure and vacuum bag. The structures are jammed using a vacuum pump with 0.85 bar. A set of 3 samples are tested for each module. The same procedure is followed at 70 °C to find out their mechanical properties in the rubbery stage. The tests are conducted to investigate the differences between the properties and behaviour of modules. After unloading the structures and modules, the core structure tends to return back to its original shape at room temperature. However, the recovery
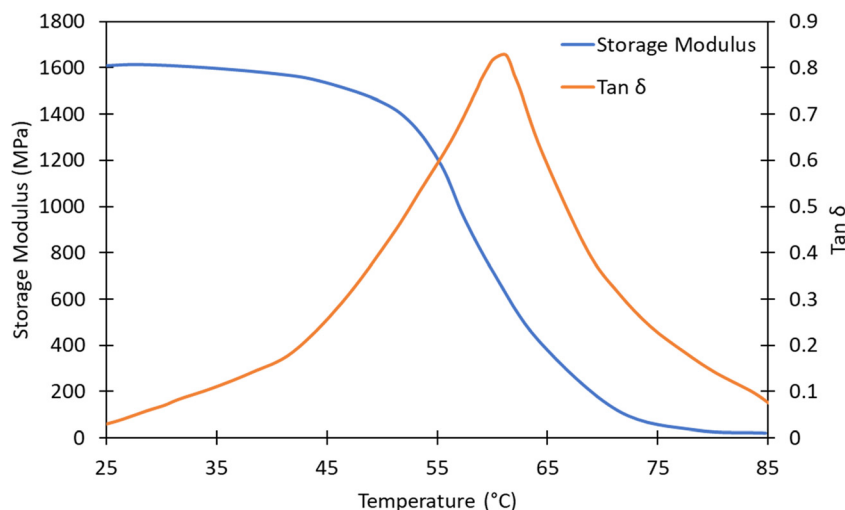

Fig. 4 Results of the DMA measurements for the printed SMP in terms of the storage modulus and tan δ.
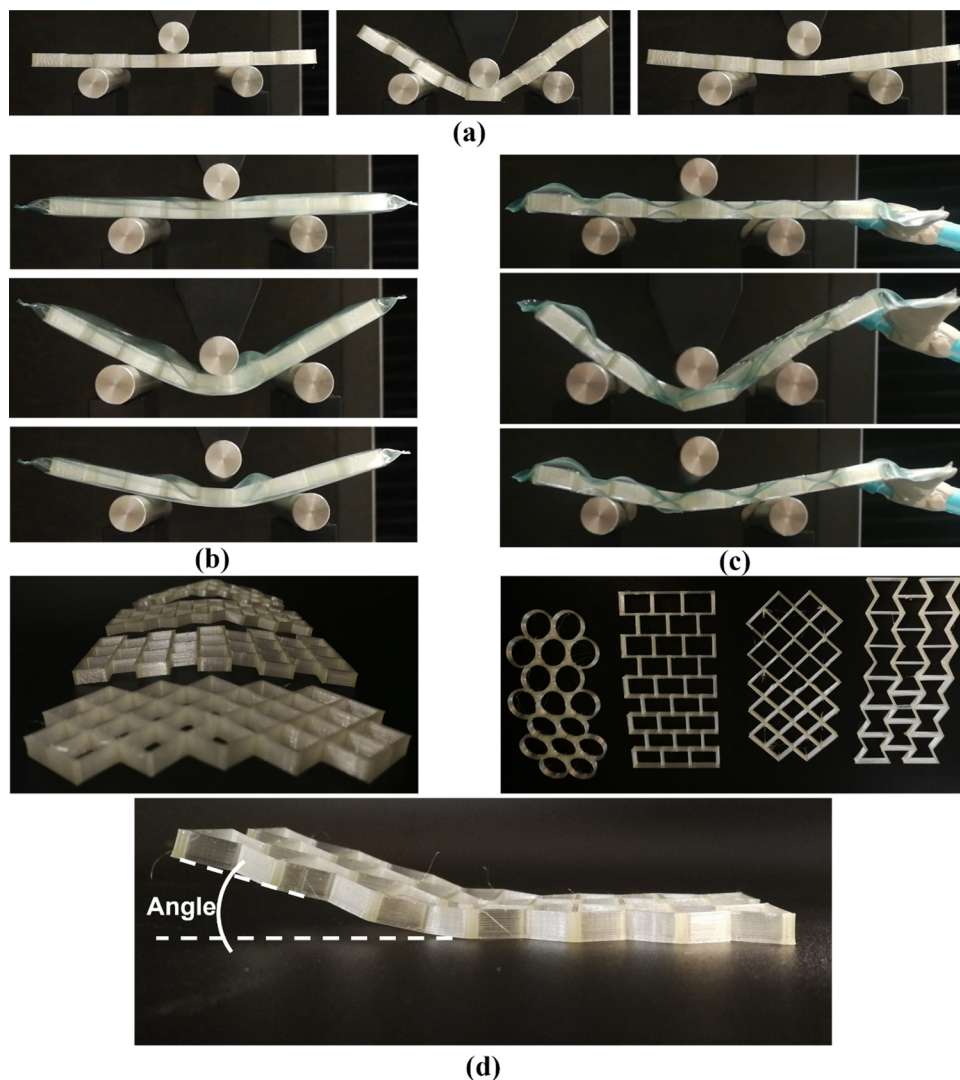
Fig. 5 Three-point bending test of (a) meta-structures, (b) unjammed MLJ with PVC sheets, and (c) jammed MLJ actuators without PVC sheets. (d) Shape recovery of meta-structures after three-point bending test.

shape is not 100% as shown in Fig. 5(d). The angle is measured for all structures to find out the differences in shape recovery after unloading.

Modules are tested under constant conditions. Several core designs with more complex deformation capabilities are investigated. Fig. 6 illustrates the behaviour of each metamaterial structure and module. Since the structure is rigid in the glassy state, the core structure plays an important role in the MLJ actuator when the shape is locked. The cyclic load graphs of auxetic, circle, diamond, and rectangle structures and modules are obtained through a three-point bending test, respectively. The force is increased to 75.11 N at 6 mm displacement and decreased to 62 N at 10 mm stroke when the core structure is auxetic and the actuator is vacuumed, see Fig. 6(a). However, when the temperature is increased the generated force decreases sharply to 1 to 2 N. The generated force is reduced since the structure is in the rubbery phase at high temperatures.[39,40] The same pattern is followed for the whole module when it is not

vacuumed, and it shows that the actuators rely on the core structure. Meanwhile, by applying negative pressure to the MLJ actuator, the actuator becomes stiff at high temperatures. However, the generated force drops under this condition since the structure is not as stiff as in the the glassy phase. Also, the results illustrate that no energy is absorbed by structures since they are in the rubbery stage.

Similar results are obtained for circle and diamond structures as shown in Fig. 6(b) and (c). However, the rectangle structure shows a different pattern. The load increases gradually up to 10 mm without a drop in force as shown in Fig. 6(d). The generated force in structures alone and structures with PVC and vacuum bags is almost equal. This means that the actuators are dependent on the core structure. Hence, controlling the core metamaterial structure leads to better performance during the stimulation. However, when the module without a PVC sheet is vacuumed, the produced load is higher accordingly. The module becomes stronger when the pump starts vacuuming the
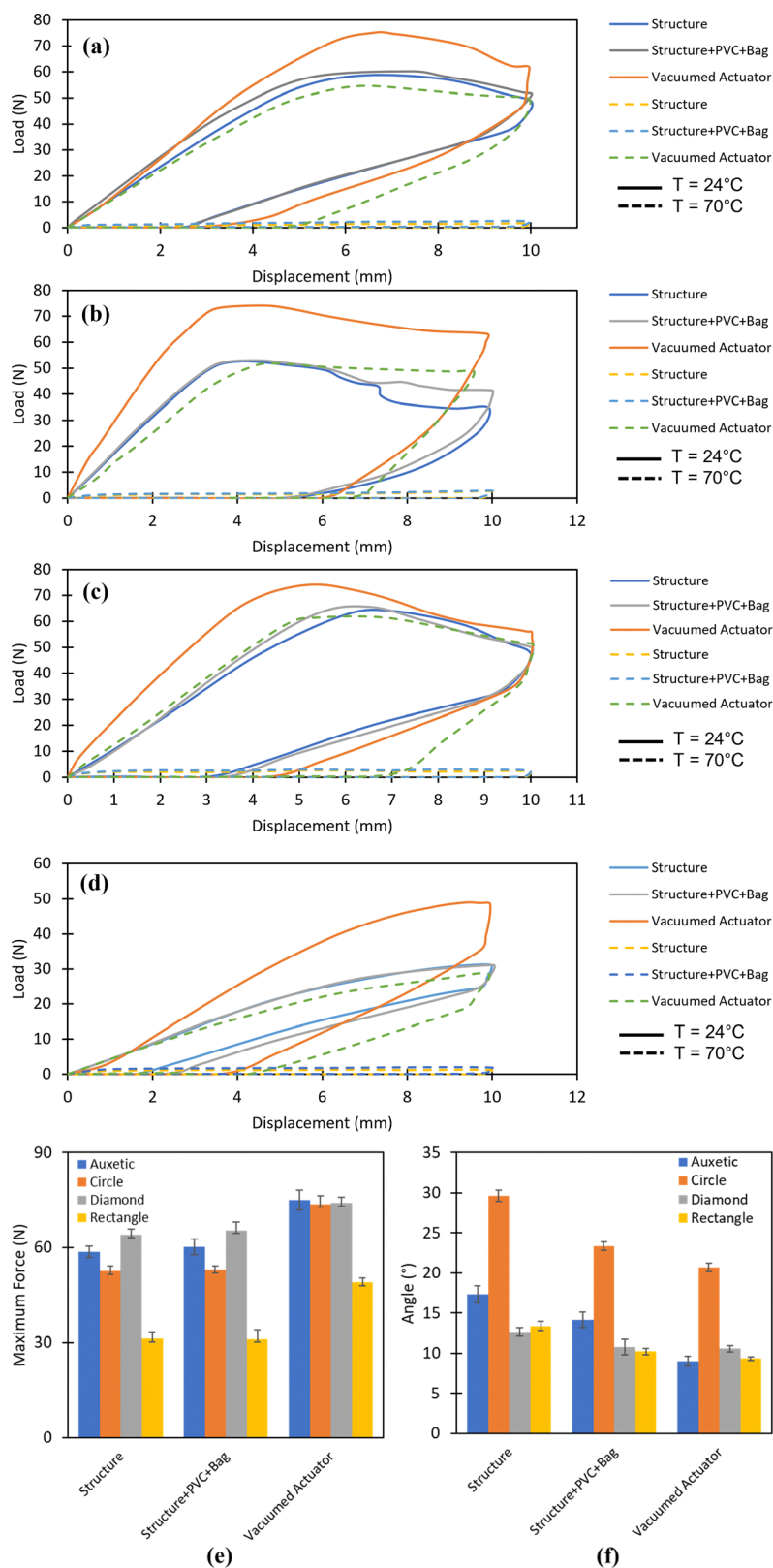
Fig. 6 Load *versus* displacement of (a) auxetic, (b) circle, (c) diamond, and (d) rectangle meta-structures and MLJ actuators at room temperature and 70 °C. (e) Obtained maximum force for different designs. (f) Obtained angle after unloading the load in the three-point bending test at room temperature.

actuators and jams the structure. The structures show an elastoplastic behaviour within a 10 mm stroke.

Fig. 6(e) shows the maximum generated force within a 10 mm stroke in all structures. The force increases in all

modules when negative pressure is applied. However, modules with PVC sheets and vacuum bags show almost the same maximum force compared to the structures alone. The applied negative pressure makes the module stiffer which affects the structure after unloading. The maximum force is almost similar for circle, auxetic, and diamond meta-structures with a value of 74 ± 1 N except for the rectangular specimens for which the value is 49.01 ± 1 N. This happens due to the cell behaviours that help absorb energy accordingly.[5,41] The absorbed energy in this area leads to better shape recovery after unloading.

Fig. 6(f) shows the obtained angle of meta-structures after unloading. The experiment is carried out to understand the performance of meta-structure shape recovery after unloading and *via* heating. Also, the angle is measured after unloading to find out how PVC films and vacuum procedure affect the core structure. The shape recovery improves after unloading when a PVC sheet or negative pressure is applied compared to structures alone. The highest values are obtained for circle-shaped structures which are $29.67 \pm 0.7°$ for the meta-structure alone and $20.67 \pm 0.5°$. When 0.85 bar negative pressure is applied, the deformation is reduced by 47% accordingly. The obtained angle for the auxetic core actuators is $9.02 \pm 0.6°$. Rectangle- and auxetic-shaped modules show better performance when the negative pressure is applied to the module in three-point bending tests. Alternately, the use of PVC sheets with high flexibility to create MLJ actuators aids in reducing the meta-structure deformation while no changes are observed in the generated force.

Other structures show the same behaviour as the auxetic structure when the temperature rises. The Young's modulus of structures drops after T_g and they lose their stiffness. Hence, the generated force is around 1 to 2 N within 10 mm displacement. However, on applying negative air pressure to the actuator module, the actuator becomes stiffer and the load increases accordingly. The frictional coefficient between internal parts, the input vacuum pressure, and the core thickness may all be optimised to increase the yield strength. However, minimum force is the main aim of this study. The main goal is to have a structure which can be bent and contracted easily with less force. Also, shape recovery is important in actuators after activation. But altering the design parameters could lead to several problems. Using a thicker core structure or PVC sheets could lead to consumption of more energy to activate the actuator.

3.2. Compression test

The compression test is conducted to evaluate the performance of meta-structures in terms of contraction in actuator modules. If the contraction in the actuator becomes high, the shape recovery of the actuator will not be 100%. Hence, the compression test is limited to 10% strain to investigate their properties. The main aim is to find out which meta-structure shape can distribute force throughout the structure and avoid concentrated force. This helps the module to contract better, and the shape recovery ratio can be higher since the force is distributed throughout the entire structure. Each sample is set up on the testing device's fixed bottom plate, and the cross-head is moved downward at a constant speed of 5 mm min^{-1} while a displacement-controlled quasi-static mechanical force is applied to the auxetic structures. Structures are anticipated to display an elastic and elastoplastic behaviour due to the low stroke. In terms of force and displacement, mechanical responses of all meta-structures are evaluated at room temperatures of 24 °C and 70 °C. In the compression test, 10% of length stroke is delivered to the SMP meta-structures.

Fig. 7(a)–(d) shows the behaviour of meta-structures under compression load at room temperature. The specimens are loaded up to 10% of their length and unloaded accordingly. As can be seen, all structures distribute the force throughout the entire structure except the circle-shaped meta-structures. A variety of pattern arrangements can exhibit various mechanical characteristics as seen in Fig. 7(e). The auxetic-shaped meta-structures appear to lose stability and undergo a softening snap-through sort of buckling after a 3 mm stroke. However, the auxetic structure contracts in both the vertical and horizontal axes.

In fact, the auxetic structure contracts laterally and vertically as the external indenter further compresses the meta-structure in the vertical direction, and material flows into the collision location to create a denser structure with a higher collision resistance. Meanwhile, the upper side of the circle-shaped meta-structure is deformed, and the applied force is concentrated on the upper side of the structure.

In this area, rectangle and diamond-shaped structures show an elastic behaviour. The meta-structure largely returns to its former shape, but certain stresses in the auxetics persist, suggesting energy loss from the plastic deformation. As a result, some of the input energy resulting from the external force is dissipated *via* the plastic deformation mechanism and is converted into kinetic energy. The stiffness of the circular unit cells in comparison to the other structures is supported by the fact that the curve slope in the elastic and plastic regions is higher than that of other structures. This means the circular meta-structure is deformed and shape recovery after unloading is not high enough. Meanwhile, the force is reduced to almost 1.5 N in all structures when the temperature goes up. The energy absorption ability of these structures is lost due to a significant reduction in their Young's modulus to 35 MPa. The strain is limited to 10 mm since the contraction of the core structure is controlled in actuators by negative pressure. All structures show almost the same trend as the three-point bending test.

Fig. 7(f) shows the maximum force for all meta-structures to investigate their stiffness accordingly. The lowest recorded force is for diamond-shaped meta-structures with a value of 102.94 ± 7.09 N followed by auxetic and rectangle structures with the values of 132.08 ± 6.02 N and 139.45 ± 7.2 N, respectively. The strongest structures among others are circle-shaped lattices with force values of 183.98 ± 6.4 N.

The obtained results from three-point bending and compression tests reveal that the circle-shaped cellular structures do not show good performances compared to others in the contraction and bending behaviour. Larger angles are obtained
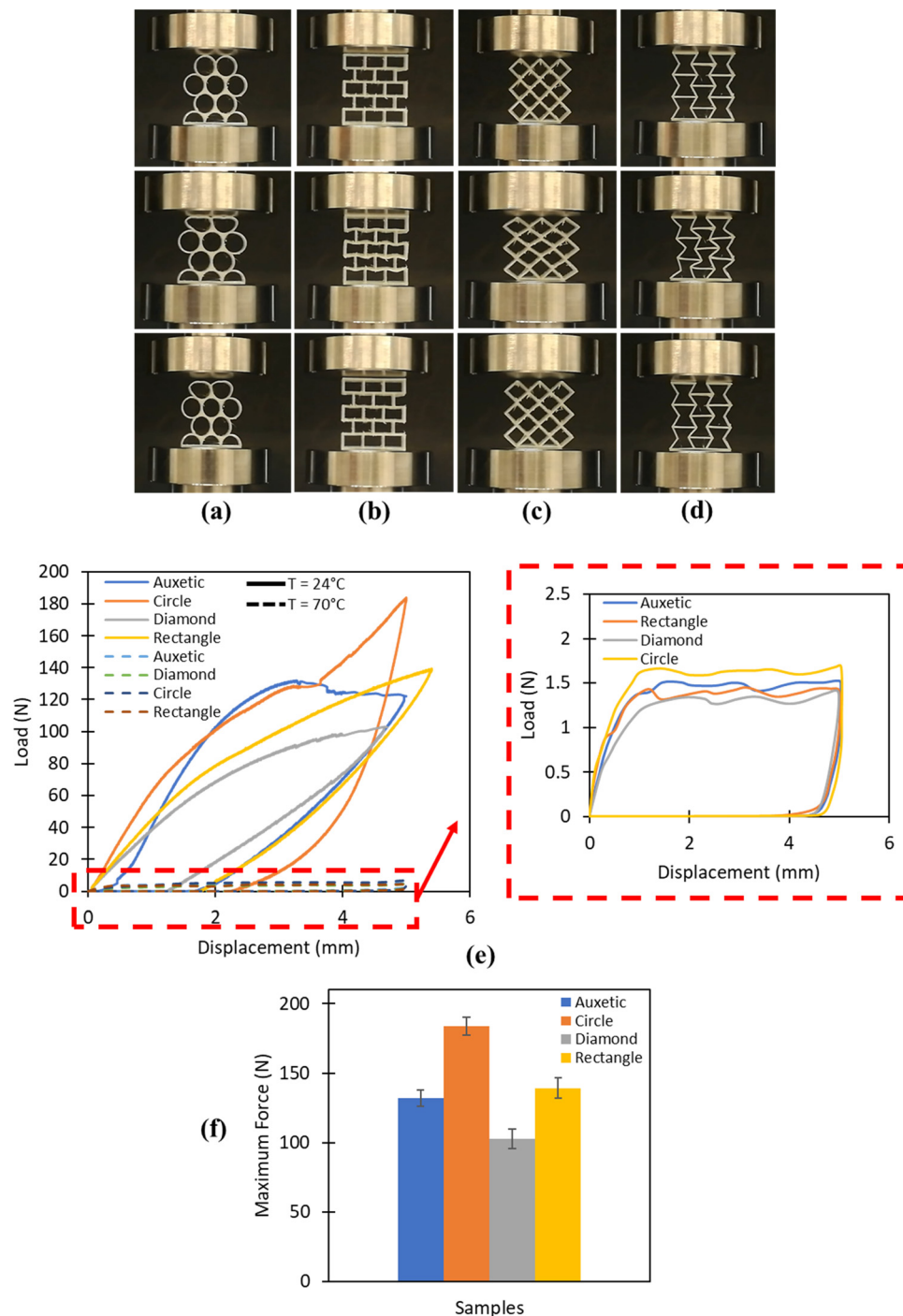
Fig. 7 Behaviour of (a) circle, (b) rectangle, (c) diamond, and (d) auxetic meta-structures under cyclic compression load. (e) Load *versus* displacement of meta-structures under one cyclic compression load at room temperature and 70 °C. (f) Obtained maximum force within 10% strain for all designs.

from circle-shaped cellular structures under the same three-point loading condition. Also, the structure is stiffer, which is not required in this study, with poor shape recovery after the cyclic compression test.

3.3. Shape memory effects

Auxetic, rectangle, and diamond meta-structures are chosen to investigate their shape recovery behaviour in terms of

contraction and bending. The test is carried out to investigate the shape recovery of core metastructures. The procedure is started by heating the structures over 60 °C which is the T_g of the polyurethane SMP material. Meta-structures are compressed when they are in the rubbery stage and then cooled down accordingly. The length of the contracted structures is measured. The specimens are heated to investigate their shape recovery features.
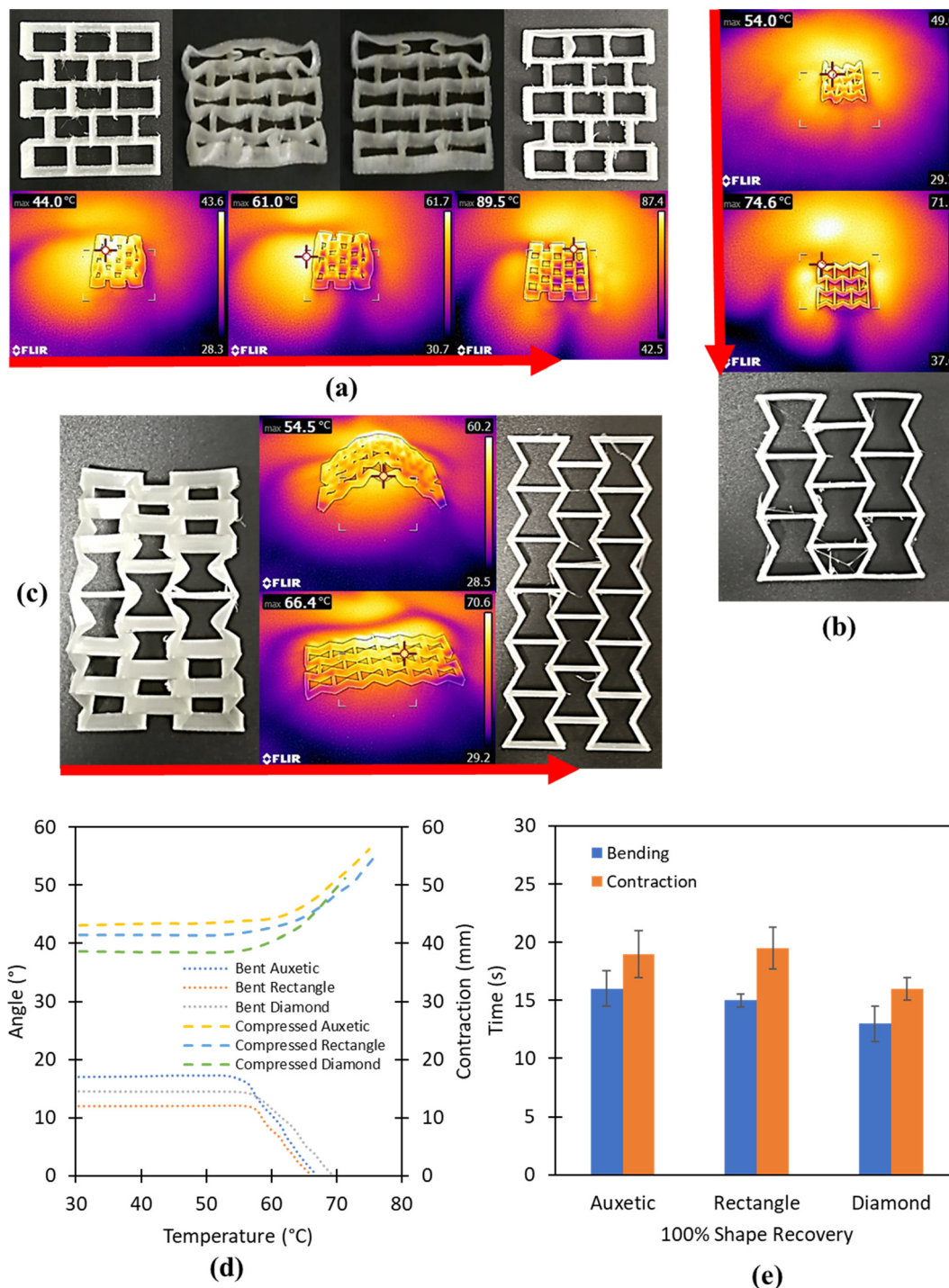
Fig. 8 (a) Procedure of shape recovery after contraction for rectangle-shaped meta-structures. The printed specimen is heated and compressed. Then, the compressed structure is heated to recover its original form. (b) Auxetic-shaped meta-structures shape the recovery procedure after contraction. (c) Procedure of shape recovery of the auxetic structure after three-point bending test unloading. (d) Shape recovery after three-point bending and compression tests for a set of specimens. (e) Recovery time of all structures when 100% shape recovery is achieved.

Fig. 8(a) illustrates the rectangle-shaped meta-structure in its original shape. The sample is compressed and cooled. The structure is heated, and the shape recovery is recorded accordingly. The structure goes back to its initial form with a shape recovery ratio of 100%. The shape recovery stages of the auxetic meta-structure are also demonstrated in Fig. 8(b). The specimen goes to its original form when the temperature reaches 74.6 °C.

Moreover, the structures are bent to evaluate the shape recovery. The bending procedure is accomplished by heating

Paper

the structure and applying load on it. A maximum angle of 30° is achieved for all meta-structures. The shape recovery of the auxetic meta-structure is shown in Fig. 8(c). The structure is heated up to 66.4 °C and the shape recovery procedure is recorded. The samples are fully recovered in the meantime. The same procedure is conducted for other structures. All meta-structures fully recover after the heating procedure using a heat gun. The heated structures show a hyperelastic behaviour and complex structures can be achieved when they are heated above T_g; however, increasing the temperature will melt the specimens or affect the SME.

Fig. 8(d) presents all structures' contraction and bending recovery after compression and the three-point bending tests. Specimens start recovering their shape as soon as the temperature reaches 60 °C. The bent meta-structures with different obtained angles after the three-point bending tests recover their shape accordingly. Also, the same procedure is conducted for compressed meta-structures. The maximum temperature at which the structures recover their shape is around 71 ± 2 °C for compressed ones and 68 ± 2 °C for bent specimens. The behaviour of the auxetic structure is different from others due to its mechanical properties and zero Poisson's ratio in terms of absorbing energy.[42] The recovery time of all meta-structures is recorded as reported in Fig. 8(e). The time is considered from the start of the heating procedure until the meta-structures fully recover. Different values are obtained due to the various angles after the three-point bending test.

All structures recover in less than 20 seconds from bent or contracted conditions. The diamond-shaped structure shows the fastest shape recovery, with 13 seconds in bending and 16 seconds under contracted conditions, respectively. However, it is possible to decrease the time by increasing the heating rate. The meta-structure properties and shape recovery are examined accordingly. The designs are used as core structures in actuators to investigate their behaviour in terms of contraction and bending.

3.4. MLJ actuators

Auxetic, rectangle, and diamond meta-structures are chosen to be used as a core in pneumatic actuators. The assembled actuators are evaluated through contraction and bending tests. Fig. 9(a) shows the procedures of stimulating the MLJ actuator with an auxetic meta-structure core. The actuator cannot be contracted or bent when the core structure is in the glassy phase. The activation of the core structure can be performed using hot water or hot air. The temperature is much higher than T_g due to the plastic cover. The heat conductivity of the plastic bag is low, and it does not allow the structure to convert to the rubbery phase if the temperature is low. Hence, the actuator is heated with a heat gun to reach 80 °C.

The MLJ actuator is heated for 30 to 35 seconds to have a uniform phase. However, heating the structure can be faster if the heating rate is higher. A negative air pressure is applied to the actuator with a maximum value of 0.4 bar. The actuator is contracted because of the core structure's softness. Subsequently, the actuator is cooled down to less than 50 °C. The contracted
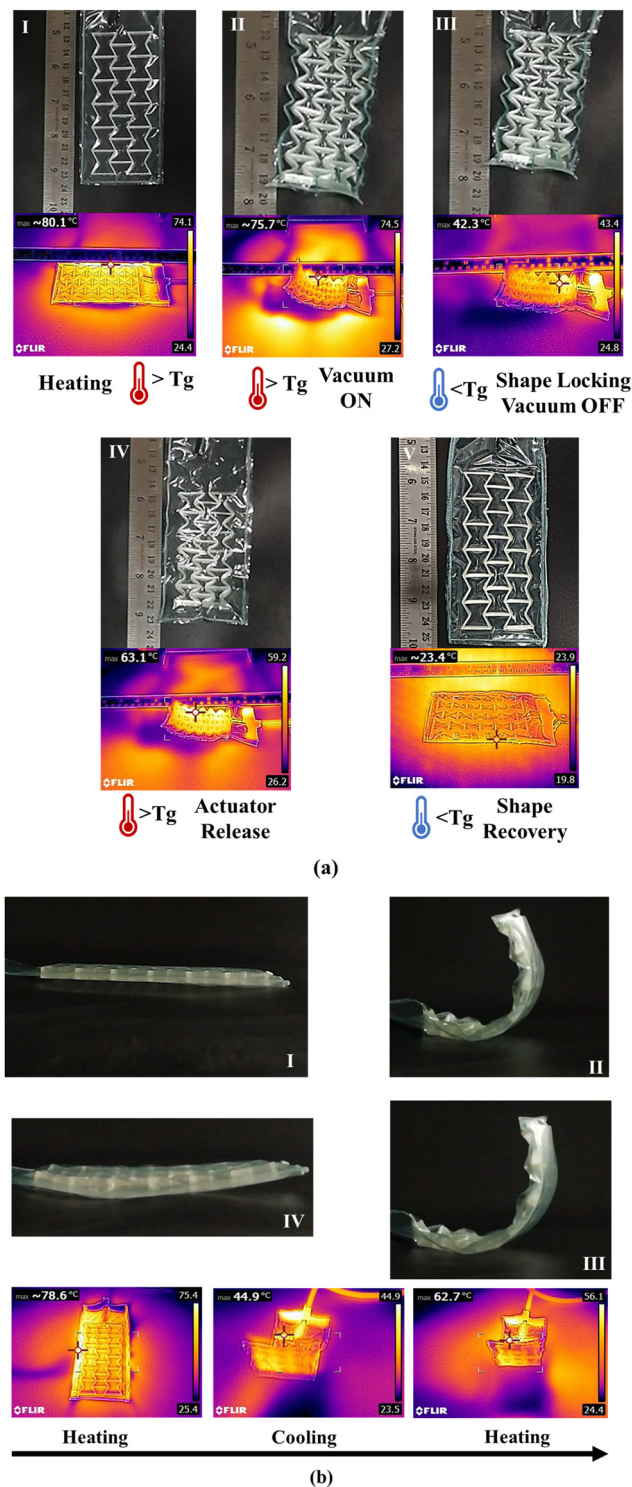

Fig. 9 Procedure of MLJ activation, shape locking without input power, and shape recovery under (a) contraction and (b) bending conditions.

actuator is locked, and the vacuum supply is turned off. The actuator can recover its original form as discussed. The actuator is released, and the power supply is removed. The structure is heated again up to 80 °C and the core structure goes back to its initial form. The shape recovery happens, and the structure is cooled down to room temperature.

The MLJ actuators have the capability to bend as well. Fig. 9(b) shows the stages of actuator's bending. The same procedures as contraction are followed for bending. However, a PVC sheet is used on one side of the core structure to bend it properly. The actuator is heated, and the power supply is started to vacuum the actuator during stage II. The actuator's shape is locked during stage III. The final stage is the shape recovery of the actuator. The actuators bend and achieve different values. The same procedure is conducted on diamond and rectangle actuators as well to evaluate their performance accordingly.

Actuators can be stimulated with high negative pressure up to 0.8 bar or thicker core metastructures. However, the deformation is high, and the core structure is not able to recover its original form completely. The contraction of the actuator is higher with 0.8 bar negative air pressure compared to 0.4 bar. However, the core structure is not able to recover its shape completely. This means that the accuracy and precision of MLJ actuators decrease in cyclic tests. Also, the twisting and deformation of the actuator during the vacuum procedure are high, which affects the results.

An alternative way to activate the structure is to turn on the vacuum power supply first. Then, the structure is heated step by step. Hence, the structure is under a negative pressure of 0.4 bar and the temperature is increasing slightly, so the actuator starts contracting or bending. However, the speed of bending and contraction is much lower compared to the first way.

A comparison is conducted among all MLJ actuators to find out the differences. The effects of core structures on MLJ actuators are investigated to find out the best core structure accordingly. A maximum negative pressure of 0.4 bar is applied to all structures throughout the tests. Shape recovery in bending and contraction tests are recorded as well. Fig. 10(a) illustrates the actuators' contraction from 0 to 0.4 bar. The contraction in the auxetic actuator is higher among others. The maximum obtained value for the auxetic-shaped core is 30 mm while it is 25 mm and 21 mm for rectangle-shaped and diamond-shaped actuators, respectively (see Fig. 10(b)). When the negative pressure reaches 0.4 bar, the contraction becomes stable until the shape locking happens. As mentioned, the contraction can be higher in all actuators if the applied negative pressure becomes more. However, the shape recovery would not be 100%.

Fig. 10(b) gives information on the generated force by MLJ actuators. There is a linear relationship between contraction and the generated force. Higher contraction results in a higher force. The maximum forces are recorded for all MLJ actuators accordingly. The maximum force for the actuator with an auxetic core structure is close to 8 N while it reduces as the contraction decreases for actuators with rectangle and diamond cores.

Fig. 10(c) shows the measurement of the tip bending angle for MLJ actuators. Increasing the negative pressure results in a higher tip angle. The tip angle of actuators is around 60° and it increases on increasing pressure (see Fig. 10(d)). The maximum tip angle with a value of 120° is for the actuator with an auxetic core when the applied negative pressure is 0.4 bar. The same negative pressure is applied to actuators with rectangle and diamond cores, and the value is 100° for both (see Fig. 10(e)).

The best performance among these actuators is for the actuator with an auxetic core due to the higher bending with the same applied negative pressure. The shape recovery of actuators in terms of contraction and bending is also evaluated. Fig. 10(f) shows the shape recovery ratio of actuators with different core structures.

Overall, the actuators show better shape recovery after bending compared to contraction. This is due to the friction between the plastic and core structure which does not allow the structure to fully recover. The shape recovery of actuators with an auxetic structure after contraction is higher compared to rectangle and diamond actuators. This happens because the auxetic core structure has zero Poisson's ratio and absorbs energy accordingly. Also, the shape recovery of actuators with an auxetic core is constant compared to others. The actuator with an auxetic structure is used to evaluate its performance in real applications. Also, the results show that the MLJ actuator is dependent on the core structure due to the different obtained angles and contractions. Also, it should be noted that on decreasing the thickness of the core structure, the actuator's performance decreases in terms of bending and contraction. This happens because of applied negative air pressure. If the core meta-structure becomes thinner the plastic covers from both sides attach to each other and block the output air. Hence, the performance of the MLJ actuator decreases accordingly.

3.5. Applications

An actuator with an auxetic structure is chosen to evaluate its performance for different applications. The schematic illustration of the procedure is shown in Fig. 11(a). The advantage of this actuator over previous LJ actuators is that continuous negative air pressure is not required to hold the MLJ during the activation stage. The actuator can be locked in the desired shape without giving input power. One side of the actuator is clamped and to the other side, the load is attached. Fig. 11(b) shows that the actuator is capable of lifting weights. The actuator is heated up to 80 °C to change the core phase from the glass phase to the rubbery phase. The power supply is started to vacuum the MLJ actuator. The actuator contracts and lifts dead weights accordingly.

The loads with the weight of 100 gr and 200 gr are applied. The MLJ actuator can lift heavy objects, but the contraction becomes lower. Also, by changing the design and applying higher negative pressure, it is possible to increase the contraction. However, shape recovery should be controlled to avoid damage and deformation. Meanwhile, the shape locking of the actuators is visible which can be a great advantage in power consumption. This advantage allows for less power consumption and makes the design more sustainable. Hence, less input pressure is required to achieve the desired shape. Also, the shape-locking feature of MLJ actuators reduces the power consumption for long-term tasks in gripping and holding.

The advantage of this MLJ actuator over previous ones is that the actuator can hold objects with zero-power input. The actuator is heated again to recover its shape. This shows that the MLJ actuator is precise enough to complete a task. Fig. 11(c) shows that the actuators can be used as a gripper to gasp and
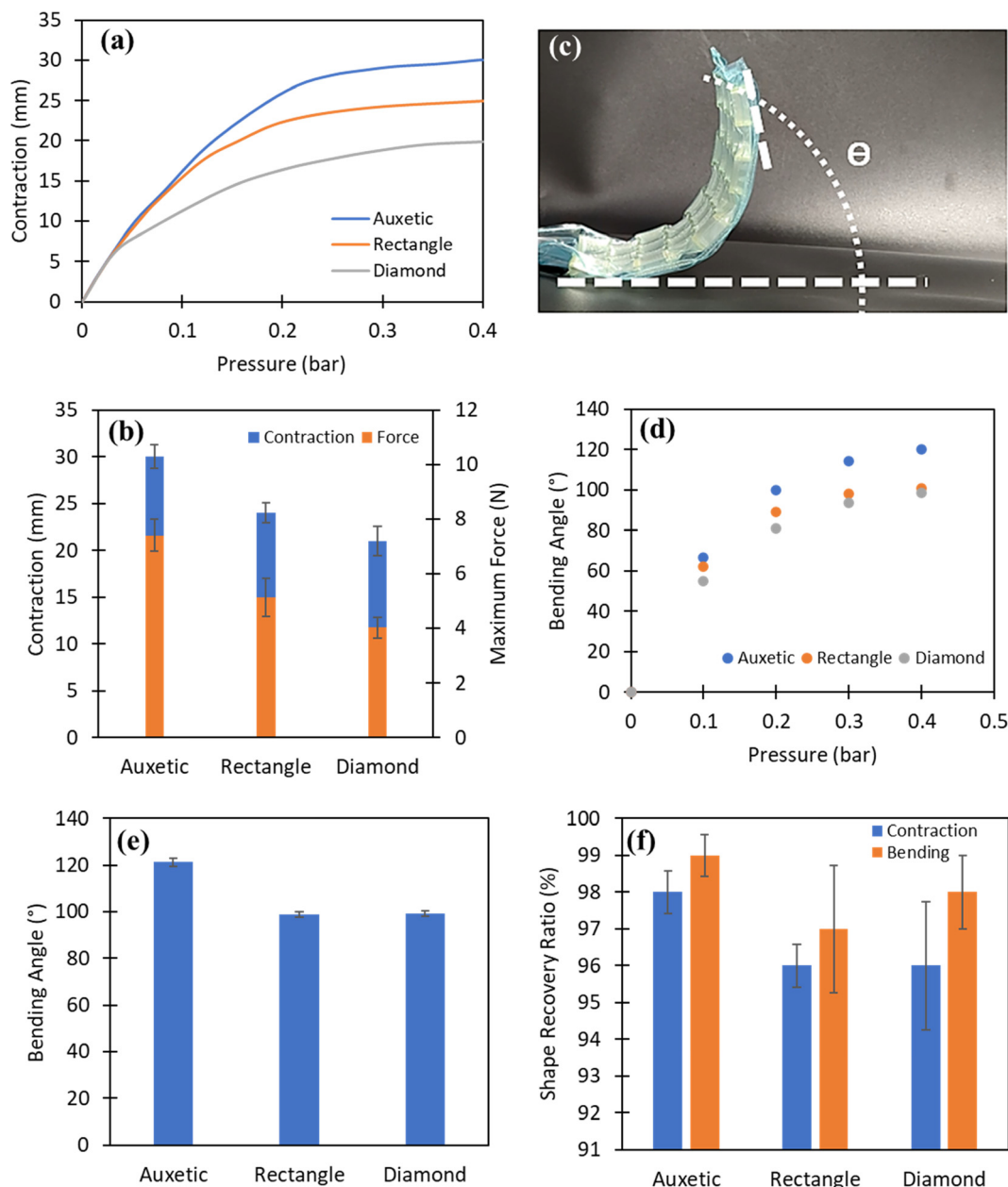
Fig. 10 (a) Behaviour of MLJ actuators in terms of contraction from 0 to 0.4 bar negative air pressure. (b) Maximum contraction and generated force for all meta-structure designs. (c) Tip bending angle measurement of MLJ actuators under locked conditions. (d) Tip angle of MLJ actuators after jamming using 0.1 to 0.4 bar negative pressure. (e) Maximum bending angle of the auxetic, rectangle, and diamond MLJ actuators after activation. (f) Shape recovery ratio of MLJ actuators after bending and contraction for all designs.

lift objects with different shore hardness without damage. Two MLJ actuators with auxetic cores and PVC sheets are clamped from one side. The actuators are heated up to 80 °C using a heat gun. A negative pressure of 0.3 bar is applied on both actuators. The actuators bend and grab the objects accordingly. The input negative pressure is turned off, and the actuator's shape is locked in the required position. By utilizing this design, zero-power holding and shape locking are attained, which are crucial because they minimize energy consumption for long-term tasks.

The performance of actuators in terms of accuracy, precision, and shape locking is investigated accordingly. Cyclic lifting is conducted with one MLJ actuator to measure its performance after a few trials. Fig. 12(a) and (b) illustrate the contraction of 5 cyclic liftings with 100 gr and 200 gr weight loads, respectively. The contraction with 100 gr loads is about 50 mm while it is around 45 mm with 200 gr. The cyclic lifting is conducted and the results are around 50 ± 2 mm and 45 ± 2 mm for 100 gr and 200 gr loads, respectively. The vacuum supply is turned off and the actuator remains
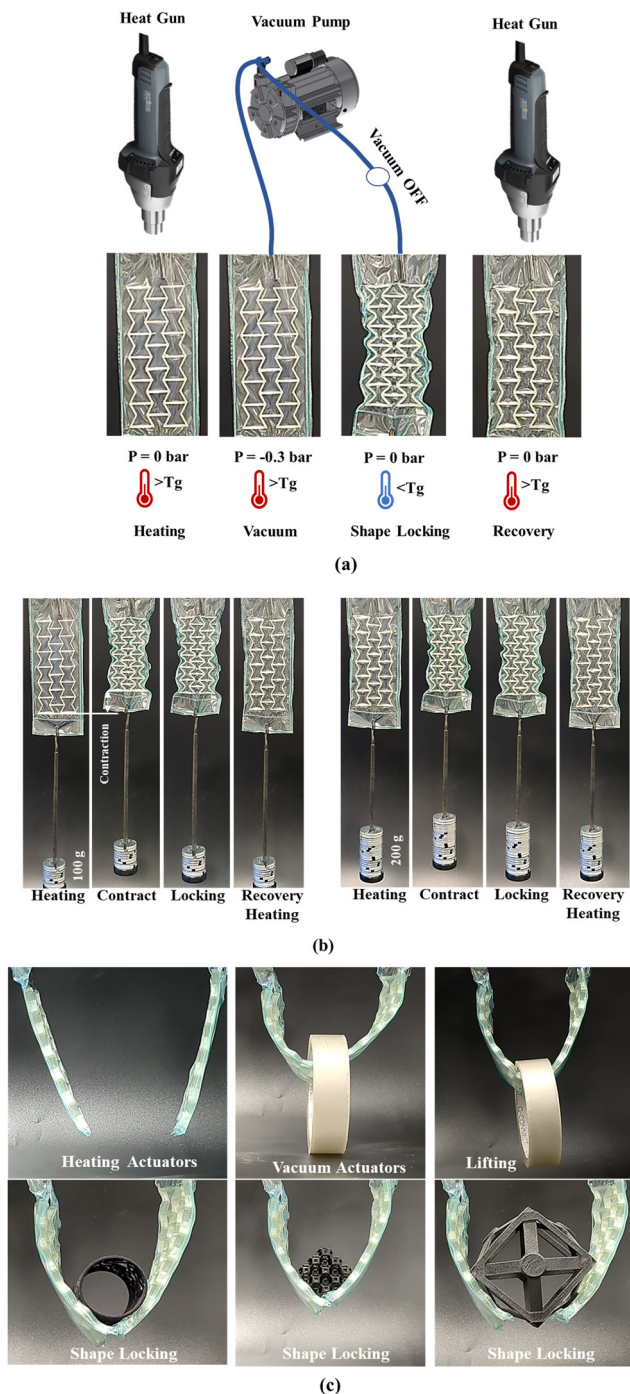
Fig. 11 (a) Schematic illustration of the MLJ actuator's activation. (b) Procedure of lifting loads with 0.4 bar negative air pressure, shape locking without power, and shape recovery of actuators. (c) Gripping and lifting objects of different weights with zero power.

in a contracted state without input power. The shape of the actuators is recovered by heating the MLJ module accordingly.

Moreover, the trajectory paths of two MLJ actuators are recorded using PASCO Capstone software. Fig. 12(c) shows the unjammed and heated jammed MLJ actuators. The jammed condition is recorded from shape-locked actuators. A target point is set to measure the repeatability and precision of both

MLJ actuators. Cyclic activation and shape recovery is conducted on both actuators for 20 cycles. As shown in Fig. 12(d), the achieved points are close to the target point with ±5 mm which shows the capability of MLJ actuators in terms of repeatability when they are activated.

The exact energy consumption will vary based on the specific design and application of the actuator. The energy consumption measurement of soft pneumatic actuators can be conducted through experiments and numerical analysis. The power consumption of a soft pneumatic actuator depends on several factors, including the pressure of the air supplied to the actuator, the size and shape of the actuator, and the desired motion and force of the actuator. In general, soft pneumatic actuators are relatively low power consumption devices, as they rely on the stored energy in compressed air to generate motion, rather than relying on electrical or mechanical power sources.[43–46]

Holding an actuator in a desired position consumes energy and power continuously. Previous works showed that a constant pressure is required to hold an actuator in the desired position for a long time.[43,44] These research works showed how much energy and power were consumed to activate the actuators. However, in this work, after activation and cooling of the MLJ actuator, no additional power is consumed to hold the actuator in the target position for long-term tasks due to the SME of the core structure. This means that the actuator does not consume energy when its shape is locked in the desired position and the vacuum pump is turned off accordingly. It is challenging to make a fair comparison of the energy consumption between different actuators, including previous models and MLJ actuators, due to the limitations posed by the specified parameters. Future research will focus on the energy consumption of MLJ actuators with the same parameters and conditions accordingly.

The shape locking and zero power holding of actuators can be used as an end-effector where the holding time is long. Meanwhile, the hot programming of this concept can be improved using electroconductive materials and thermally isolated plastic. Electroconductive materials and isolated plastics help to reduce the activation time. The heating procedure becomes easier with electroactive SMP materials as well.

4. Conclusion

This study illustrates the potential of combining 4DP and LJ technologies in soft actuator fields. A novel technique was implemented to develop MLJ actuators with shape memory behaviours and shape-locking features. Circle, rectangle, diamond, and auxetic meta-structures were developed to investigate their properties. The mechanical properties of meta-structures in terms of cyclic three-point bending and compression tests were evaluated accordingly. Shape recovery and shape memory effects of meta-structures were also investigated through bending and contraction tests. The behaviour of MLJ
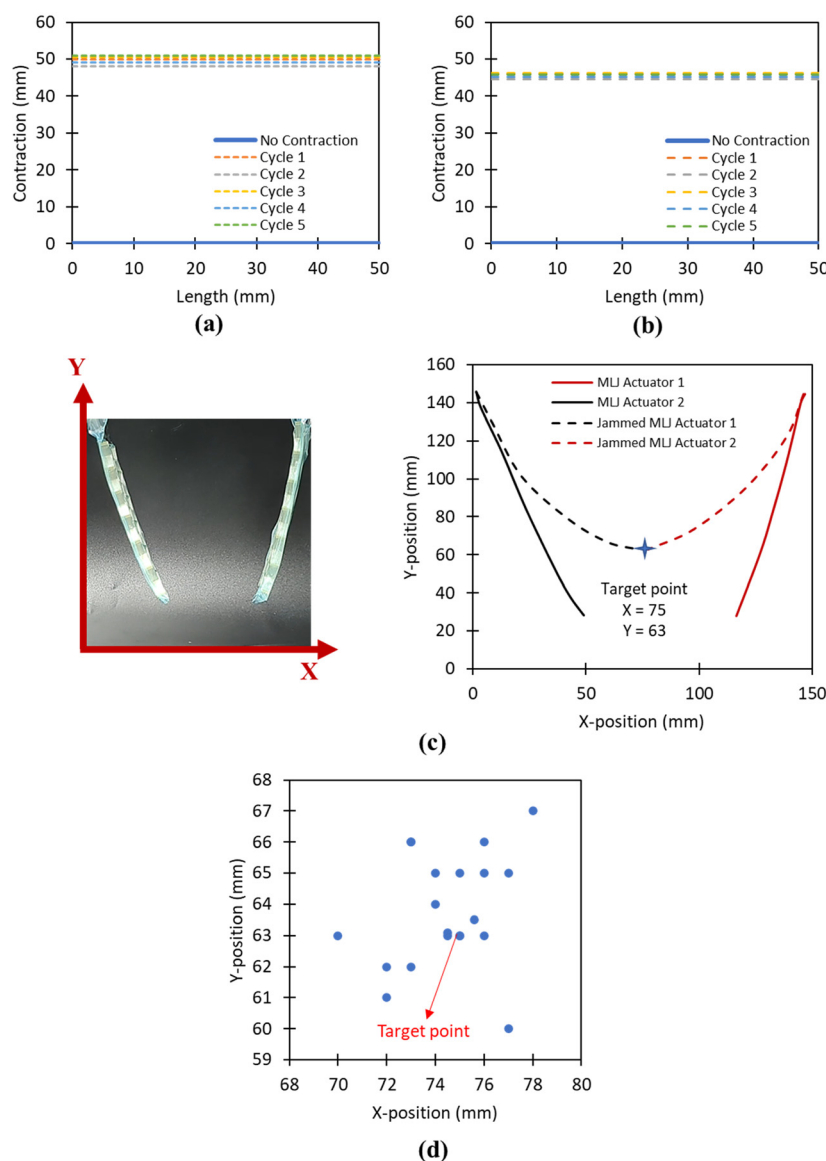
Fig. 12 Cyclic activation and contraction with (a) 100 g and (b) 200 g load. (c) Trajectory path of actuators under unjammed and shape-locking conditions. (d) Cyclic behaviour of two MLJ gripper actuators based on the target point in 20 cycles.

actuators was investigated in terms of contraction and bending under applied negative pressure. The results revealed that MLJ actuators with auxetic meta-structures perform better in bending, contraction, and shape recovery among others. Shape-locking features, zero-power holding, and gripping are the main features of the developed actuator. Collectively, the work clarifies the physics of LJ and 4DP, speeds up the construction of jamming actuators, and establishes a basis for building mechanically adaptable actuators and meta-structures which can be sustainable due to less power consumption.

Author contributions

MLD and MB contributed to the conceptual design, methodology, investigation, and validation. MLD performed material preparation, data collection and analysis. MLD wrote the first draft of the manuscript and MB revised and commented on all versions of the manuscript. MLD and MB read and approved the final manuscript. The authors gratefully acknowledge use of the services and facilities at Nottingham Trent University.

Conflicts of interest

There are no conflicts to declare.

References

1 D. Rus and M. T. Tolley, Design, fabrication and control of soft robots, *Nature*, 2015, **521**, 467–475, DOI: **10.1038/nature14543**.

2 X. Dong, X. Luo, H. Zhao, C. Qiao, J. Li, J. Yi, L. Yang, F. J. Oropeza, T. S. Hu, Q. Xu and H. Zeng, Recent advances in biomimetic soft robotics: fabrication approaches, driven strategies and applications, *Soft Matter*, 2022, **18**, 7699–7734, DOI: **10.1039/D2SM01067D**.

3 M. Lalegani Dezaki, M. K. A. Mohd Ariffin and S. Hatami, An overview of fused deposition modelling (FDM): research, development and process optimisation, *Rapid Prototyp J.*, 2021, **27**, 562–582, DOI: **10.1108/RPJ-08-2019-0230**.

4 M. Bodaghi, A. R. Damanpack and W. H. Liao, Adaptive metamaterials by functionally graded 4D printing, *Mater. Des.*, 2017, **135**, 26–36, DOI: **10.1016/j.matdes.2017.08.069**.

5 M. Bodaghi, A. Serjouei, A. Zolfagharian, M. Fotouhi, H. Rahman and D. Durand, Reversible energy absorbing meta-sandwiches by FDM 4D printing, *Int. J. Mech. Sci.*, 2020, **173**, 105451, DOI: **10.1016/j.ijmecsci.2020.105451**.

6 Y. Cao, X. Feng, S. Wang, Q. Li, X. Li, H. Li, W. Hong, H. Duan and P. Lv, Multiple configuration transitions of soft actuators under single external stimulus, *Soft Matter*, 2022, **18**, 8633–8640, DOI: **10.1039/D2SM01058E**.

7 J. Qi, Z. Chen, P. Jiang, W. Hu, Y. Wang, Z. Zhao, X. Cao, S. Zhang, R. Tao, Y. Li and D. Fang, Recent Progress in Active Mechanical Metamaterials and Construction Principles, *Adv. Sci.*, 2022, **9**, 2102662, DOI: **10.1002/advs.202102662**.

8 W. Wu, W. Hu, G. Qian, H. Liao, X. Xu and F. Berto, Mechanical design and multifunctional applications of chiral mechanical metamaterials: A review, *Mater. Des.*, 2019, **180**, 107950, DOI: **10.1016/j.matdes.2019.107950**.

9 M. Lalegani Dezaki, M. Bodaghi, A. Serjouei, S. Afazov and A. Zolfagharian, Adaptive reversible composite-based shape memory alloy soft actuators, *Sens. Actuators, A*, 2022, **345**, 113779, DOI: **10.1016/j.sna.2022.113779**.

10 J. Delaey, P. Dubruel and S. van Vlierberghe, Shape-Memory Polymers for Biomedical Applications, *Adv. Funct. Mater.*, 2020, **30**, 1909047, DOI: **10.1002/adfm.201909047**.

11 F. Meder, G. A. Naselli, A. Sadeghi and B. Mazzolai, Remotely Light-Powered Soft Fluidic Actuators Based on Plasmonic-Driven Phase Transitions in Elastic Constraint, *Adv. Mater.*, 2019, **31**, 1905671, DOI: **10.1002/adma.201905671**.

12 M. Lalegani Dezaki, M. Bodaghi, A. Serjouei, S. Afazov and A. Zolfagharian, Soft Pneumatic Actuators with Controllable Stiffness by Bio-Inspired Lattice Chambers and Fused Deposition Modeling 3D Printing, *Adv. Eng. Mater.*, 2023, 2200797, DOI: **10.1002/adem.202200797**.

13 Y.-F. Zhang, Z. Li, H. Li, H. Li, Y. Xiong, X. Zhu, H. Lan and Q. Ge, Fractal-Based Stretchable Circuits *via* Electric-Field-Driven Microscale 3D Printing for Localized Heating of Shape Memory Polymers in 4D Printing, *ACS Appl. Mater. Interfaces*, 2021, **13**, 41414–41423, DOI: **10.1021/acsami.1c03572**.

14 A. le Duigou, G. Chabaud, F. Scarpa and M. Castro, Bioinspired Electro-Thermo-Hygro Reversible Shape-Changing Materials by 4D Printing, *Adv. Funct. Mater.*, 2019, **29**, 1903280, DOI: **10.1002/adfm.201903280**.

15 Y. Cao and J. Dong, Programmable soft electrothermal actuators based on free-form printing of the embedded heater, *Soft Matter*, 2021, **17**, 2577–2586, DOI: **10.1039/D0SM02062A**.

16 A. Zolfagharian, S. Gharaie, A. Z. Kouzani, M. Lakhi, S. Ranjbar, M. Lalegani Dezaki and M. Bodaghi, Silicon-based soft parallel robots 4D printing and multiphysics analysis, *Smart Mater. Struct.*, 2022, **31**, 115030, DOI: **10.1088/1361-665X/ac976c**.

17 C. Yang, F. Su, Y. Liang, W. Xu, S. Li, E. Liang, G. Wang, N. Zhou, Q. Wan and X. Ma, Fabrication of a biomimetic hydrogel actuator with rhythmic deformation driven by a pH oscillator, *Soft Matter*, 2020, **16**, 2928–2932, DOI: **10.1039/C9SM02519G**.

18 A. Zolfagharian, A. Kaynak, S. Y. Khoo and A. Kouzani, Pattern-driven 4D printing, *Sens. Actuators, A*, 2018, **274**, 231–243, DOI: **10.1016/j.sna.2018.03.034**.

19 M. Lalegani Dezaki and M. Bodaghi, Soft Magneto-Responsive Shape Memory Foam Composite Actuators, *Macromol. Mater. Eng.*, 2022, **307**, 2200490, DOI: **10.1002/mame.202200490**.

20 M. Lalegani Dezaki and M. Bodaghi, Magnetorheological elastomer-based 4D printed electroactive composite actuators, *Sens. Actuators, A*, 2023, **349**, 114063, DOI: **10.1016/j.sna.2022.114063**.

21 M. Y. Khalid, Z. U. Arif, W. Ahmed, R. Umer, A. Zolfagharian and M. Bodaghi, 4D printing: Technological developments in robotics applications, *Sens. Actuators, A*, 2022, **343**, 113670, DOI: **10.1016/j.sna.2022.113670**.

22 E. Yarali, M. Baniasadi, A. Zolfagharian, M. Chavoshi, F. Arefi, M. Hossain, A. Bastola, M. Ansari, A. Foyouzat, A. Dabbagh, M. Ebrahimi, M. J. Mirzaali and M. Bodaghi, Magneto-/electro-responsive polymers toward manufacturing, characterization, and biomedical/soft robotic applications, *Appl. Mater. Today*, 2022, **26**, 101306, DOI: **10.1016/j.apmt.2021.101306**.

23 S. G. Fitzgerald, G. W. Delaney and D. Howard, A Review of Jamming Actuation in Soft Robotics, *Actuators*, 2020, **9**, 104, DOI: **10.3390/act9040104**.

24 Y. Wang, L. Li, D. Hofmann, J. E. Andrade and C. Daraio, Structured fabrics with tunable mechanical properties, *Nature*, 2021, **596**, 238–243, DOI: **10.1038/s41586-021-03698-7**.

25 D. Hwang, E. J. Barron, A. B. M. T. Haque and M. D. Bartlett, Shape morphing mechanical metamaterials through reversible plasticity, *Sci. Robot.*, 2022, **7**, DOI: **10.1126/scirobotics.abg2171**.

26 B. Yang, R. Baines, D. Shah, S. Patiballa, E. Thomas, M. Venkadesan and R. Kramer-Bottiglio, Reprogrammable soft actuation and shape-shifting *via* tensile jamming, *Sci. Adv.*, 2021, **7**, DOI: **10.1126/sciadv.abh2073**.

27 B. Aktaş, Y. S. Narang, N. Vasios, K. Bertoldi and R. D. Howe, A Modeling Framework for Jamming Structures, *Adv. Funct. Mater.*, 2021, **31**, 2007554, DOI: **10.1002/adfm.202007554**.

28 Y. Gao, X. Huang, I. S. Mann and H.-J. Su, A Novel Variable Stiffness Compliant Robotic Gripper Based on Layer Jamming, *J. Mech. Robot.*, 2020, **12**(5), 051013, DOI: **10.1115/1.4047156**.

29 W.-B. Li, X.-Y. Guo, F.-Y. Fang and W.-M. Zhang, Amplifying Laminar Jamming for Soft Robots by Geometry-Induced

Rigidity, in: 2021 IEEE International Conference on Robotics and Automation (ICRA), IEEE, 2021: pp. 11907–11912, DOI: **10.1109/ICRA48506.2021.9561415**.

30 M. Ibrahimi, L. Paternò, L. Ricotti and A. Menciassi, A Layer Jamming Actuator for Tunable Stiffness and Shape-Changing Devices, *Soft Robot.*, 2021, **8**, 85–96, DOI: **10.1089/soro.2019.0182**.

31 Y. S. Narang, J. J. Vlassak and R. D. Howe, Mechanically Versatile Soft Machines through Laminar Jamming, *Adv. Funct. Mater.*, 2018, **28**, 1707136, DOI: **10.1002/adfm.201707136**.

32 Y. Lin, G. Yang, Y. Liang, C. Zhang, W. Wang, D. Qian, H. Yang and J. Zou, Controllable Stiffness Origami "Skeletons" for Lightweight and Multifunctional Artificial Muscles, *Adv. Funct. Mater.*, 2020, **30**, 2000349, DOI: **10.1002/adfm.202000349**.

33 J. Kwon, I. Choi, M. Park, J. Moon, B. Jeong, P. Pathak, J. Ahn and Y. Park, Selectively Stiffening Garments Enabled by Cellular Composites, *Adv. Mater. Technol.*, 2022, **7**, 2101543, DOI: **10.1002/admt.202101543**.

34 X. Wang, L. Wu, B. Fang, X. Xu, H. Huang and F. Sun, Layer jamming-based soft robotic hand with variable stiffness for compliant and effective grasping, *Cognit. Comput. Syst.*, 2020, **2**, 44–49, DOI: **10.1049/ccs.2020.0003**.

35 Y. S. Narang, A. Degirmenci, J. J. Vlassak and R. D. Howe, Transforming the Dynamic Response of Robotic Structures and Systems Through Laminar Jamming, *IEEE Robot. Autom. Lett.*, 2018, **3**, 688–695, DOI: **10.1109/LRA.2017.2779802**.

36 L. Gerez, G. Gao, A. Dwivedi and M. Liarokapis, A Hybrid, Wearable Exoskeleton Glove Equipped With Variable Stiffness Joints, Abduction Capabilities, and a Telescopic Thumb, *IEEE Access*, 2020, **8**, 173345, DOI: **10.1109/ACCESS.2020.3025273**.

37 N. Willemstein, H. van der Kooij and A. Sadeghi, 3D printing of soft fluidic actuators with graded porosity, *Soft Matter*, 2022, **18**, 7269–7279, DOI: **10.1039/D2SM00524G**.

38 F. Wang, F. Luo, Y. Huang, X. Cao and C. Yuan, 4D Printing *Via* Multispeed Fused Deposition Modeling, *Adv. Mater. Technol.*, 2022, 2201383, DOI: **10.1002/admt.202201383**.

39 R. Tao, L. Ji, Y. Li, Z. Wan, W. Hu, W. Wu, B. Liao, L. Ma and D. Fang, 4D printed origami metamaterials with tunable compression twist behavior and stress-strain curves, *Composites, Part B*, 2020, **201**, 108344, DOI: **10.1016/j.compositesb.2020.108344**.

40 R. Tao, L. Xi, W. Wu, Y. Li, B. Liao, L. Liu, J. Leng and D. Fang, 4D printed multi-stable metamaterials with mechanically tunable performance, *Compos. Struct.*, 2020, **252**, 112663, DOI: **10.1016/j.compstruct.2020.112663**.

41 R. Hamzehei, A. Zolfagharian, S. Dariushi and M. Bodaghi, 3D-printed bio-inspired zero Poisson's ratio graded metamaterials with high energy absorption performance, *Smart Mater. Struct.*, 2022, **31**, 035001, DOI: **10.1088/1361-665X/ac47d6**.

42 A. Yousefi, S. Jolaiy, M. Lalegani Dezaki, A. Zolfagharian, A. Serjouei and M. Bodaghi, 3D-Printed Soft and Hard Meta-Structures with Supreme Energy Absorption and Dissipation Capacities in Cyclic Loading Conditions, *Adv. Eng. Mater.*, 2022, 2201189, DOI: **10.1002/adem.202201189**.

43 Y. Shengda, T. Wang and S. Zhu, Research on energy consumption of fiber-reinforced fluidic soft actuators, *Smart Mater. Struct.*, 2021, **30**, 025036, DOI: **10.1088/1361-665X/abd7e6**.

44 J. Luo, P. Jiang, X. Li, L. Bai, F. Liu and R. Chen, A Soft Self-Stable Actuator and Its Energy-Efficient Grasping, *Actuators*, 2022, **11**, 107, DOI: **10.3390/act11040107**.

45 B. Vanderborght, B. Verrelst, R. van Ham, M. van Damme, D. Lefeber, B. M. Y. Duran and P. Beyl, Exploiting Natural Dynamics to Reduce Energy Consumption by Controlling the Compliance of Soft Actuators, *Int. J. Robot. Res.*, 2006, **25**, 343–358, DOI: **10.1177/0278364906064566**.

46 M. Wehner, M. T. Tolley, Y. Mengüç, Y.-L. Park, A. Mozeika, Y. Ding, C. Onal, R. F. Shepherd, G. M. Whitesides and R. J. Wood, Pneumatic Energy Sources for Autonomous and Wearable Soft Robotics, *Soft Robot.*, 2014, **1**, 263–274, DOI: **10.1089/soro.2014.0018**.